Humanoid robotic arm design with S-R-S configuration, redundant swivel angles analysis, and collision-free trajectory planning

Yi-Hao Zhu, Hsien-Ting Chang, and Jen-Yuan (James) Chang

Abstract— In recent years, high-DOFs robotic arms have been investigated for various labor force shortage applications, such as welding and assembling, because of the brought flexibility. High-DOFs configuration can reduce the occurrence of the singularity and bring the possibility of optimization. However, it becomes more unintuitive for neophytes to operate. To compensate for this drawback, transferring human arm movements directly to the robot is more intuitional. For this purpose, the mechanical design of the humanoid robotic arm to meet the simplified kinematic model of the human is presented first in this research. Furthermore, the redundant characteristics of the 7-DOF humanoid robotic arm were analyzed to optimize the endeffector's manipulability by adjusting swivel angles without changing the position and the orientation of the end-effector. Last, obstacle avoidance was also considered and achieved by using the oriented bounding box, which can decrease the computation time and provides the closest collision point with obstacles. The result shows that the mechanism can mimic human-like motions, and the algorithm can optimize the manipulability and the obstacle-free trajectory.

Index Terms— Humanoid robotic arm, manipulability, obstacles avoidance, oriented bounding box, swivel angle.

I. INTRODUCTION

ince high-DOFs robotic arms have become an essential part of flexible manufacturing system (FMS), the robot's mechanism and corresponding optimized strategies in operations evidentially need to adapt to various applications to match the manufacturing flexibility. Contrary to commonly used 6-DOFs industrial robots require more stiffness, preciseness, and maximum velocity. The critical aspect of using high-DOFs robotic arms is to allow transferring of human skills more intuitively in numerous tasks. The simplest high-DOFs robotic arm model is a serial mechanical chain with 7-DOFs [1], and this structure is adopted in this research. In addition to the high-DOFs of the robotic arm for FMS, flexibility in the robot arm's end0effector is also critical. The design of an endeffector that is in the form of the human hand is adopted in the present study not only because it is more relevant to the modal problem but also because its structure can provide adaptation to

The authors appreciate the supported by the Ministry of Science and Technology of Taiwan under Grant MOST 108-2218-E-007-025 for the work. Yi-Hao Zhu¹, Hsien-Ting Chang², and Jen-Yuan (James) Chang³ are both with the Department of Power Mechanical Engineering National Tsing Hua

University, Hsinchu City, Hsinchu County 30013, Taiwan.

objects being grasped. This design can provide an intuitive control interface with the 7-DOFs robotic arm to mimic human whole-arm grasping movement.

The German Aerospace Centre (DLR) has been working on 7-DOFs serial robot arms since the 1990s and transferred this technology to the KUKA Robot Group in 2004. Since then, several commercial robotic arms [2-4], as listed in TABLE I, have been developed. Although it is motivated by human arm and control strategies that may be perfect for the 7-DOFs serial robot, their objective was not to design humanoid robots but merely to add one more DOF to the existing 6-DOFs industry robots. In the robot's last two degrees of freedom, the pitch-roll configuration is chosen for applications using tools, such as drilling operations, for instance. Each joint is offset by a linear distance to increase the moving range, and the whole length of the robotic arm is often longer than the human arm, intending to reach a bigger working space. Thus, to mimic the whole-arm grasping movement, it is necessary to change the traditional mechanical design [5, 6] for the 7-DOFs serial robot in this study.

TABLE I ROBOTIC ARMS

REFERENCE	ROBOTIC ARM	COMPANY
[2]	UR5	Universal Robots
[3]	JACO	Kinova
[4]	LBR iiwa	KUKA

Besides the kinematics model fitting the anthropomorphic structure, the control method also needs to be developed. Moreover, human-like path planning can facilitate human-robot collaboration. Since human beings can predict the corresponding robot's motions, they may adjust their actions to avoid possible collisions or even to enhance the partnership between the human and the robot. To achieve this goal, the direct use of the actual demonstrations of a human being as a reference is commonly seen in literature [7]. The precise coordination between the robot's joint movements brings about human-like movements. But the quality of the demonstration is usually found to be inconsistent. The length of the real arm not

(E-mail: ¹arsenezhu@gapp.nthu.edu.tw, ²htchang@gppp.nthu.edu.tw, ³jychang@pme.nthu.edu.tw).

being equal to the mechanical structure of the robot is one of the reasons. Therefore, there must be an optimized method to solve this problem. There are plentiful techniques and strategies to optimize human moves, such as facilitated imitation learning and kinematics methods [8, 9]. Imitation learning depends on estimating the peculiarities of the demonstrated motion in a task or joint configuration. This method collects anthropometrical data from massive experiments and then analyzes the data to form a model, such as the regression model. This method is suitable for people intuitively solving the problem and generating motion data from task inputs. However, its drawback is a lack of generality. What's worse is that thousands of experiments need to be conducted over and over when tasks and the environment change. It not only wastes vast amounts of time but also needs more careful demonstration to get better results.

Since humans naturally can minimize unknown objective functions during performing tasks, correspondingly, human movement can be investigated by applying optimization approaches with the appropriate cost function [10, 11]. Kinematics methods apparently use knowledge about human arm kinematics and biomechanics to solve the joint trajectories by optimizing the performance index and considering the joint constraints. The resolution of this approach is much better than the former one as it offers better repeatability. However, the performance index needs to be chosen carefully and must be proficient in Denavit-Hartenberg (D.H.) coordinate system. In the case of a redundant robotic arm with more than 6 DOFs, its inverse kinematics provide several or infinite solutions. To account for human arm movement, the natural approach is to apply the anthropomorphism criterion to the infinite solutions to reach solutions of human-like movements. Conventionally, the optimized approaches, like minimizing the traveled distance and avoiding singularity, seem to be not enough [12-14]. In this research, we explore manipulability [15], standing for the mobility for the end-effector in the current joint configuration, to figure out how it affects the robotic hand's efficient grasping posture by increasing the major-axis alignment manipulability.

While reaching the grasping posture, collision avoidance must be considered in motion planning. For the computation of the distance between obstacle and robot, in literature, geometry bounding methods [16] are commonly adopted. Which method is hierarchically organized to simplify the robot's contact region. One of the bounding methods is the bounding sphere method. This method checks the distance between the centers of robot structures and obstacles to decide whether the collision can occur or not. If it is less than the sum of their radii, then the collision happens. Approximating the model with more spheres can improve collision detection accuracy, but the trade-off is the computational resources [17]. In this research, instead of the bounding-sphere method, we apply a bounding-box method to fit the collision region of the robot's linkage at once. Not only does it meet the actuator's appearance, but it also can increase the calculation speed. Finally, the avoidance direction is decided by generating the virtual force with the vector of the

collision point and center of the obstacle.

Since the mechatronics and coordinate systems for the human-like robotic arm are proposed, developed, and discussed in this paper, the kinematics methods are first adopted as the backbone of the study. The contents of this paper addressing the research divides into three-part. The first part is about the mechanical design based on the anthropometric studies of the human arm, consisting of the shoulder, elbow, and wrist. We map the motion data directly collected from humans into the robotic arm to ensure the feasibility of the mechanical design. In the second part, the 7-DOFs joint coordinate system is constructed by applying the D.H. method. An optimized method with maximization of the major-axis alignment criterion is proposed. In the third part, we validate the obstacleavoiding algorithm in a robot simulator without the issue of interference with hardware. The objective of this research aims at creating a mechatronic system, including a humanoid robotic arm having 7-DOFs and a human-like motion planning algorithm. The organization of this paper is therefore structured as follows. Section 2 shows the anthropomorphic mechanism design. Section 3 discusses the optimized process. Section 4 applies the obstacle-avoiding algorithm to motion planning. Section 5 demonstrates the feasibility of mechanical design by directly mapping the motion data collected from humans and proposing a performance index to accomplish the pouring task. Finally, conclusions are drawn in Section 6.

II. ANTHROPOMORPHIC MECHANISM DESIGN

This research presents a mechanical design of the humanoid robotic arm to meet the simplified kinematics model of the human arm and thus can transfer human arm movements directly to the robot arm. The human arm consists of 7 joints. The first 3 joints' axes are perpendicular to each other to form a spherical joint, and so do the last 3 joints to form the spherical wrist joint. It is found in practice that the traditional model of 7-DOFs serial robots in the industry suffers from gimbal lock problems when imitating human wrist motion. The gimbal lock causes the system to rotate in a degenerate space, so the moving range of the end-effector is less than usual. To implement the spherical trajectory movement of the human's wrist, the rotational axes of the last two DOFs must intersect at one point, and these axes need to be orthogonal to the forearm's axis. An assembly of the first DOF, the pitch, and the second DOF, the yaw, therein offer an ability to mimic human wrist motion. This research provides insight by discussing two versions of the wrist mechanism based on the pitch-yaw configuration and demonstrates the pros and cons in engineering practices.

A modular wrist design can connect the mechanical joint between the hand and wrist. As shown in Fig.1, the first version is inspired by Cheng-Yu's method [6]. Their work provides a compact wrist design based on two coupled four-bar linkages and two motors fixed at the structure of the forearm. This design achieves a human-like appearance and obtains a high gear ratio by a ball screw. However, its nonlinear dynamic behavior of coupling four-bar linkages was observed to cause problems in positioning when operated at high speed. This problem can cause the trajectory following the operation of the end-effector (hand) to fail. Inspired by Rosheim's design concept, the second

version is illustrated in Fig. 2. The actuators for the second DOF (yaw) are located directly at the joint without any offset. This design makes the drive unit quite simple, and the response time from the motor to the linkage is shorter than in the former model. Since the design priority is placed on short response time in developing a 7-DOFs humanoid robotic arm for realtime control, the second design is chosen in this research.



Fig. 1 Spherical movement of human's wrist with the first design

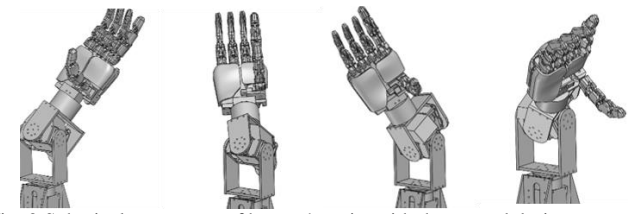


Fig. 2 Spherical movement of human's wrist with the second design

The next step is to build up the whole 7-DOFs mechatronic system. The first three DOFs of the model humanoid arm represent the shoulder, the fourth DOF indicates the elbow, and the last three DOFs mimic the forearm and wrist. The shell and the housing need to be as light as possible to save energy while executing tasks, so aluminum material was chosen. Also, the seven motors need to be controlled at the same time. Therefore bulk-reading for multiple devices is an essential requirement. Most importantly, it is vital to consider cost, so RS-485 rather than EtherCAT is selected as a communication protocol for implementing bulk-read of commands and responses from the seven motors. In this paper, the Dynamixel Pro-series motors [18] are chosen to construct the humanoid robotic arm. With the implementation of the second wrist design, the total length of the humanoid arm is decreased by 15%, and the torque transmission rate increases. The whole mechanism became more compact, and the final design of the 7-DOFs humanoid robotic arm is shown in Fig. 3.

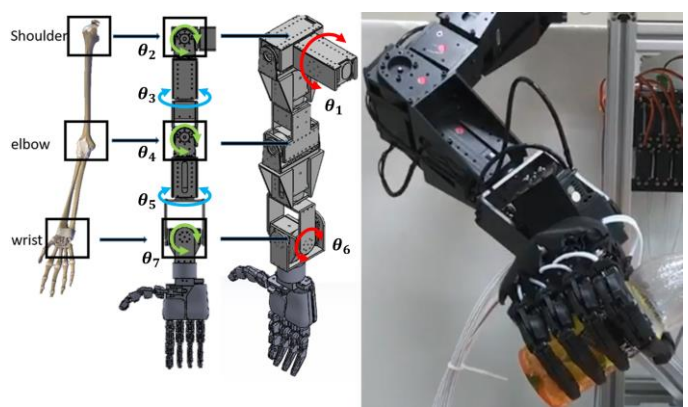


Fig. 3 Final design of 7-DOFs humanoid robotic arm.

III. KINEMATIC MODEL

The purpose of developing the 7-DOFs robotic arm is to overcome two technical shortcomings of the 6-DOFs robotic arm reported in the literature. The first is that the 6-DOFs robotic arm will not change pose without affecting the endeffector under the particular configuration. The second is the uneven and non-continuous distribution of joint displacement to reach a specific pose because only finite solutions can be calculated. Therefore, the collision between the 6-DOFs robotic arm and obstacles in the workspace cannot be avoided in some scenarios.

Since the addition of an extra one DOF to a traditional 6-DOFs robotic arm demands much in computation, motion planning of a 7-DOFs humanoid robot requires a computationally efficient approach to calculate the robot's joint configurations at a given end-effector posture. This kind of problem is known as the Inverse Kinematics (I.K.) problem. As reported in the literature, there are two categories to solve the I.K. problem. The first one is the iterative Jacobi method using Jacobian pseudoinverses after each small change in the state of the end-effector. This method uses local linearization to handle the highly nonlinear system. The second method is the analytical inverse kinematics utilizing classic trigonometric descriptions to derive the relationship between the posture of the end-effector and the joints without iterations. The second method is adopted in this research for it is able to provide an I.K. solution and decrease computation time for fast control requirements. Only six constraints, including orientation and position, are needed to reach a specific end-effector pose. We must first set one more restriction on the 7-DOFs arm in this study. The definition of redundant angle should match the goal of mimicking human arm movement. The swivel angle φ , as shown in Fig 4, is chosen as the seventh restriction because this motion is identical to human instinct movement. Before illustrating the swivel angle, the plane P_{sew} needs to be explained. This plane consists of three points: shoulder joint, elbow joint, and wrist joint. The reference plane is the formed plane after solving I.K. when the end-effector's position and orientation are given while the third joint's angle is constrained to zero. The swivel angle then is defined as the angle between the reference plane and the plane when specifying a different angle to the third joint. These two planes are coaxial with the vectors defined by the shoulder and wrist joints; this movement happens to coincide with the actual movement of the human arm.

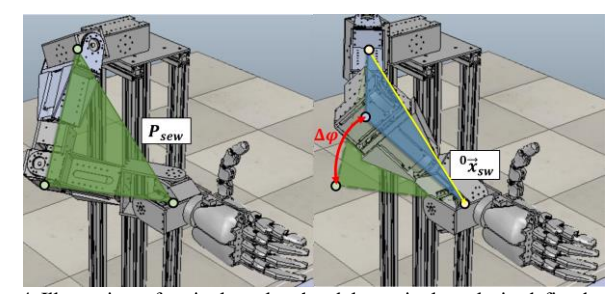


Fig. 4 Illustration of swivel angle: the delta swivel angle is defined as the difference between green and blue planes. Both planes consist of three points: shoulder, elbow, and wrist joint. Only the angle of the joint is different.

The Denavit-Hartenberg coordinate system is constructed in TABLE II, and the transformation matrix can lead to a feasible solution of I.K. using Shimizu's method [9].

 $\label{eq:table_in_table} TABLE\ II \\ DH\ parameter\ of\ the\ 7-DOFs\ robotic\ arm$

i	$\boldsymbol{\theta}$	α (rad)	d	а
1	$oldsymbol{ heta}_1$	$-\pi/2$	d_{bs}	0
2	$oldsymbol{ heta}_2$	$\pi/2$	0	0
3	θ_3	$-\pi/2$	d_{se}	0
4	$oldsymbol{ heta_4}$	$\pi/2$	0	0
5	$\boldsymbol{\theta}_{5}$	$-\pi/2$	d_{ew}	0
6	$\boldsymbol{\theta}_{6}$	$\pi/2$	0	0
7	θ_7	0	d_{wt}	0

The inverse kinematics is derived as follows. First, let ${}^{0}x_{sw}$ be the vector from the shoulder to the wrist. Because the fourth angle will not be affected by changing the swivel angle, we can compute it using (1).

$$\cos \theta_4 = \frac{\|{}^{0}x_{sw}\|^2 - d_{se}^2 - d_{ew}^2}{2 * d_{se}d_{ew}}$$
(1)

TABLE III
SYMBOL DESCRIPTION

	STMBOL DESCRIPTION				
Symbol	Description				
$^{j}R_{i}$	i th rotation matrix represented in j th coordinate				
$^{\mathrm{j}}R_{arphi}$	Rotation matrix of swivel angle represented in j th coordinate				
^j x _i	i th position represented in j th coordinate				
$^{j}l_{bs}$	Length between base to shoulder represented in j th coordinate				
$^{j}l_{se}$	Length between shoulder to elbow represented in j th coordinate				
$^{j}l_{ew}$	Length between elbow to wrist represented in j th coordinate				
$^{j}l_{wt}$	Length between wrist to target represented in j th coordinate				
v	General end-effector state vector				
θ	Vector of motor angles				
I	Jacobian matrix				

Then, we solve the other six angles in (2) and (3) by using the formal forward kinematics relationship between joint angles and pose, including the desired position ${}^{0}x_{7}$ and orientation ${}^{0}R_{7}$. The meaning of each symbol is listed in Table III.

$${}^{0}x_{7} = {}^{0}l_{bs} + {}^{0}R_{\varphi} {}^{0}R_{3}^{o} \left\{ {}^{3}l_{se} + {}^{3}R_{4} \left({}^{4}l_{ew} + {}^{4}R_{7} {}^{7}l_{wt} \right) \right\}$$
 (2)

$${}^{0}R_{7} = {}^{0}R_{\varphi} {}^{0}R_{3}^{o} {}^{3}R_{4} {}^{4}R_{7}$$
 (3)

IV. OPTIMIZED APPROACH

In the previous sections, through the analysis and verification of inverse kinematics, the 7-DOFs arm can be fully controlled. Further, the redundant degree of freedom, the swivel angle, must be optimized. The optimization goal of this research is to improve the efficiency of the grasping pose at the end-effector, which is the humanoid hand, as shown in Figs. 3 and 4. For this purpose, the relationship between motor angles and the end-effector's position and orientation must be figured out so that the Jacobian matrix can be derived. Although the position and the orientation can be calculated based on (2) and (3), the matrix form of orientation can't be partially differentiated by a vector. The pose should be transformed to three Euler angles, namely

 α , β , and γ angles, respectively, and be composed with three-position values to form a new general end-effector state vector. Thus the Jacobian matrix can be derived.

$$\dot{v} = I\dot{\theta} \tag{4}$$

$$J = \frac{\partial \dot{v}}{\partial \dot{\theta}} \tag{5}$$

Then it is necessary to calculate the manipulability for the optimization goal of this research. The greater the manipulability, the more efficient the grasping pose is. The calculation of manipulability is shown in (6).

$$\|\dot{\theta}\|^2 = \dot{\theta}^T * \dot{\theta} = \dot{v}^T (JJ^T)^{-1} \dot{v}$$
 (6)

In (6), θ represents the motor angle of the robotic arm, and J represents the Jacobian matrix. It can be known from the above formula that $M = JJ^T$ describes the manipulability of the robotic arm at the restriction of $\|\dot{\theta}\|^2 = 1$. Fig. 5 shows the manipulability changes caused by changing the swivel angle. The red ellipse is the visualized result of the manipulability matrix. In order to feedback control the motor angles to achieve the desired manipulability, it is necessary to differentiate manipulability to obtain a control gradient matrix. However, the derivative of a matrix with respect to a vector is a tensor of order 3. To simplify the calculation, the vectorization of a matrix is introduced in (7), where T represents the permutation matrix, \otimes is the Kronecker product, and j = vec(J).

$$d \operatorname{vec}(M) = \operatorname{vec}(dJJ^{T}) + \operatorname{vec}(JdJ^{T})$$

$$= (J \otimes I_{6}) * dj + (I_{6} \otimes J) * T * dj$$

$$= (I_{36} + T)(J \otimes I_{6}) * dj$$
(7)

$$\tau_{36\times7} = \frac{\partial \text{vec}(M)}{\partial \theta}$$

$$= (I_{36} + T)(J \otimes I_6) * \frac{dj}{\partial \theta}$$
(8)

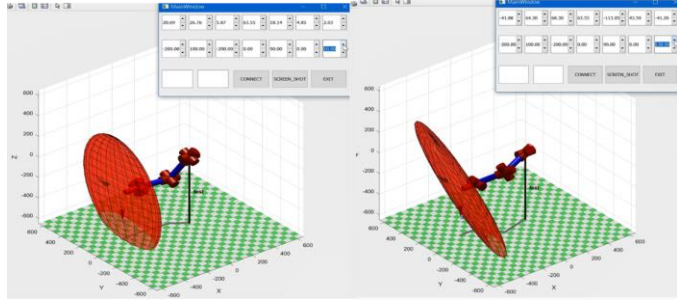


Fig. 5 Visualized result of manipulability at same end-effector position and orientation but different swivel angle

After establishing the differential relationship between manipulability and motor angle in (8), the input must be considered. The manipulability M is highly nonlinear because it is the multiplication of the Jacobian matrix. With Riemann geometry, we can compute the difference between each

manipulability matrix. This difference denoted as $L_{6\times 6}$ is defined in (9), where A and B are 6×6 manipulability matrices.

$$L_{6\times 6} = \text{Log}_A(B) = A^{\frac{1}{2}} * \log(A^{-\frac{1}{2}}BA^{-\frac{1}{2}}) A^{\frac{1}{2}}$$
 (9)

After the difference between two manipulability is calculated, the concept of the gradient descent is employed used to make manipulability asymptotically toward the target manipulability M_t .

Additionally, because the $L_{6\times 6}$ is a matrix, it should be vectorized as a 36×1 vector. This vector reflects all column vectors in $L_{6\times 6}$. Finally, the overall control method is defined in (10), in which \dot{v}_t is the target end-effector general velocity calculated during trajectory planning.

$$\dot{\theta_t} = J^{-1}(\dot{v}_t) + (I - J^{-1}J) * \tau^T * vec(L_{6 \times 6})$$
 (10)

If the robotic arm encounters a singular point and causes the elements of the Jacobian matrix to be infinite, the pseudoinverse Jacobian matrix is adopted Mathematically, the purpose of using the Jacobian matrix is to optimize the redundant degree of freedom for enlarging manipulability. In this research, we propose to combine analytical solutions to assist the Jacobian matrix in calculating the current posture. This hybrid approach for the controller is depicted in the flowchart, as shown in Fig. 6.

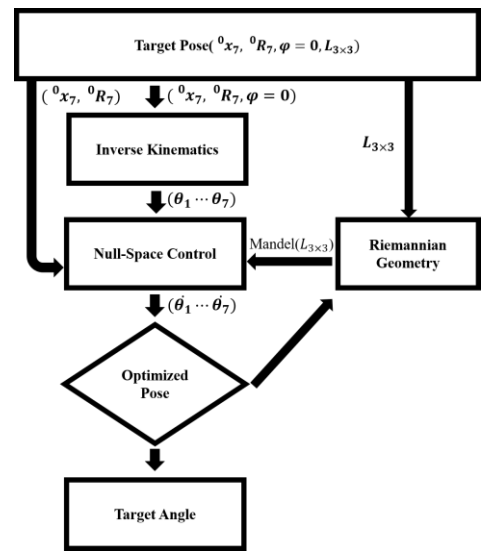
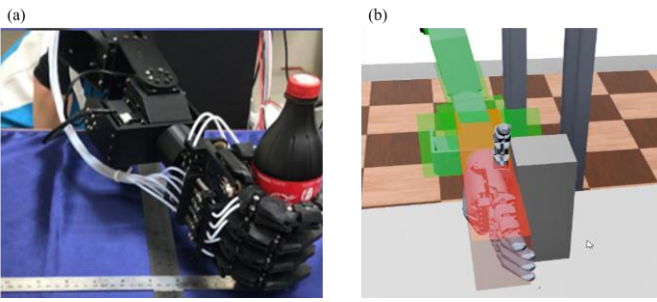


Fig. 6 Flowchart of the proposed hybrid controller

V. OBSTACLE AVOIDING STRATEGY

While reaching the grasping posture, collision avoidance must be considered in motion planning. The geometry bounding method is commonly used in the literature to compute collision between obstacle and robot. This traditional approach can improve collision detection accuracy by approximating the model with an enormous number of spheres but costs more computational resources. Instead of using spheres, in this research, the bounding-box method is employed to fit the collision region of the robot's linkage at once. Not only can it meet the actuator's appearance, but it also increases computation speed. The information regarding the collision is

provided by the bounding box of each robot linkage and the obstacles. The distances from all points on the robot linkage bounding boxes to the obstacles are then computed to figure out the closest point as the possible collision point of the robot. The avoidance direction is defined as a virtual force along the direction from the collision point to the center of the obstacle. Then null-space movements are added to avoid collision with an external obstacle. To separate algorithm and hardware issues, we develop the Webot simulation environment in this research and validate different scenarios of the robot's behavior when encountering obstacles in the workspace. The collisionfree area is marked as green. On the contrary, the collision area is then highlighted with red color.



Robotic grasp detection: (a) Real-world implementation. Simulated-world implementation.

In engineering practice, a vision system is commonly used to mark the target but inevitably suffers from occlusions. The robot linkage structures and their corresponding bounding box can be assumed to be rigid since they have higher stiffness than the interactive objects. With such a solid assumption, bounding boxes can be applied to robot structures to determine the collision with an external object and evaluate the theoretical gripping position, as shown in Fig. 7. With this remedy, we can solve occlusions. Finally, Fig. 8 shows the flowchart of the aforementioned obstacle avoidance strategy. The main task of this strategy is to update the target angles iteratively with nullspace control if the collision is detected by the OBB algorithm to obtain the proper target angles, which can be executed successfully.

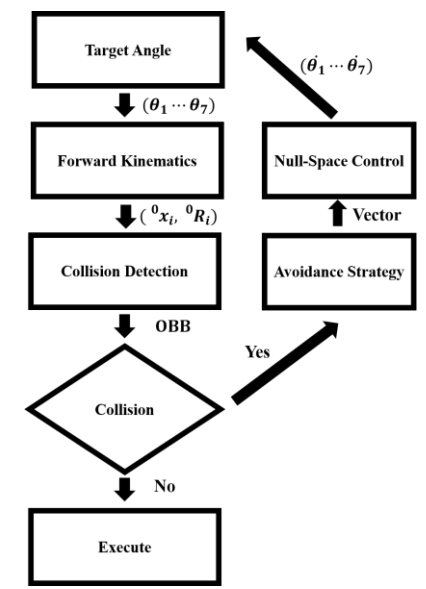


Fig. 8 Flowchart of the proposed obstacle avoidance strategy

Although the OBB method is useful and easy to be achieved, the application scenario should follow the assumptions mentioned above. When using the OBB method, any possibility that may lead mismatching phenomenon should be considered carefully, such as model difference, assembling error, or deformation during dynamic motion or interaction with other objects. Otherwise, a more margin of the bounding box needs to be included to increase the robustness but decrease the precision.

VI. EXPERIMENTAL RESULTS

With the proposed human-like robotic arm and the pitch and yaw DOFs, the ability to implement the spherical trajectory movement of the human's wrist without suffering from gimbal lock is demonstrated by the series of screen shots as shown in Fig. 9. Moreover, Fig. 10 shows the feasibility of the humanoid robotic arm by directly mapping a human's joint movement to the model robotic arm. Fig. 11 uses hand grasping tasks to demonstrate that the gimbal lock problem does not trap the wrist design. Finally, the collision-free trajectory planning algorithm with bounding boxes for the humanoid manipulator is validated in the cyber or virtual domain first. It is graphically illustrated in Fig. 12 and Fig. 13, respectively, for moving without and with obstacle avoidance. By fine-tuning the robot's PID controllers, we can implement the trajectory from the aforementioned cyber domain to the corresponding physical domain or real system. As an illustrative example, as shown in Fig. 14, the robot is set to perform a pouring task, which is more complicated and involves dexterous motion. The results show that we can smoothly perform the job by using a planning algorithm based on the proposed hybrid analytical inverse kinematics algorithm. The redundant angle during the movement apparently meets the requirement of the joint limit, force transmission, and obstacle avoidance.

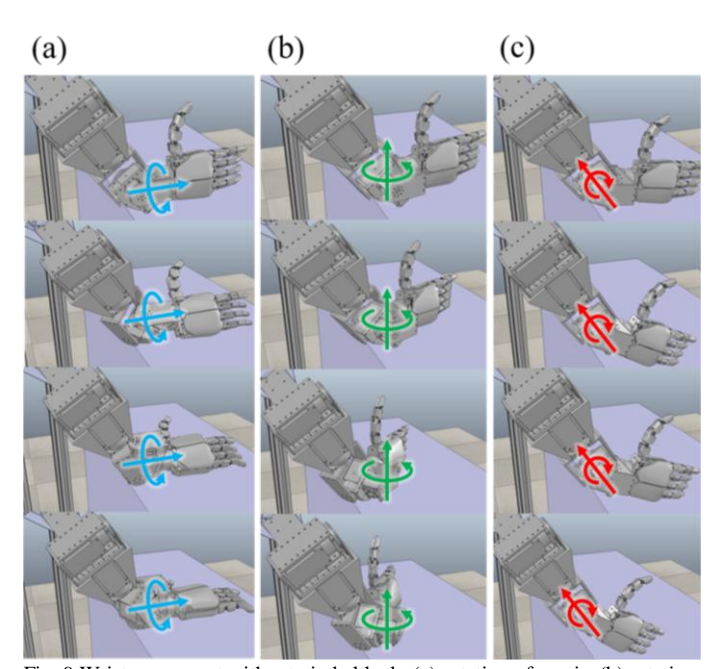


Fig. 9 Wrist movement without gimbal lock: (a) rotation of *z*-axis, (b) rotation of *y*-axis, and (c) rotation of *x*-axis.

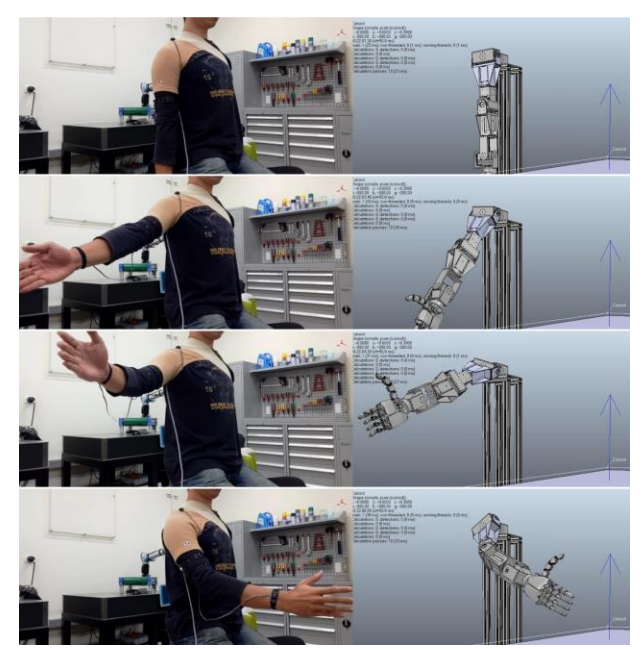


Fig. 10 The proposed humanoid robotic arm imitating human arm movement.



Fig. 11 Hand grasping of various objects

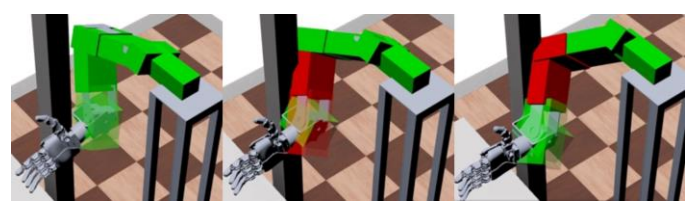


Fig. 12 Moving without obstacle avoidance

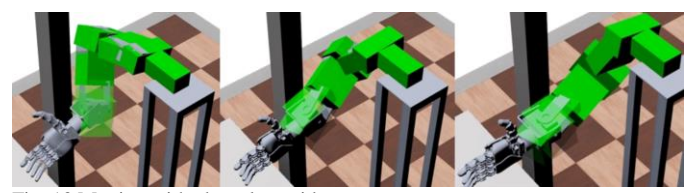


Fig. 13 Moving with obstacle avoidance.

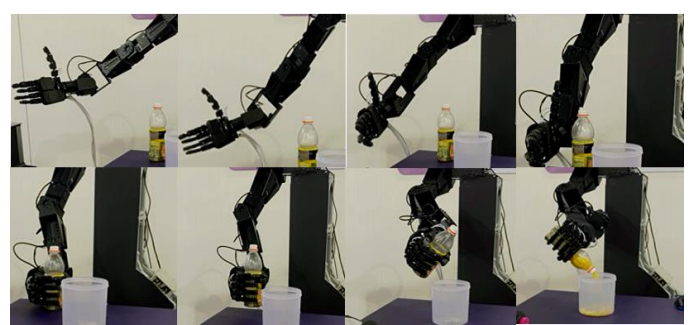


Fig. 14 Example of the model humanoid robotic arm conducting pouring task.

VII. CONCLUSION

We have proposed a hybrid inverse kinematics model with a S-R-S arm configuration, manipulability human-like optimization through adjusting the redundant swivel angles, and the ability of obstacle avoidance when performing the target grasping poses. The S-R-S configuration 7-DOF robotic arm overcomes the gimbal lock problem increasing the flexibility of the end-effector without decoupling the gimbal at first, as shown in Fig 9. Second, the manipulability optimization increases the manipulability at the same position and the orientation of the end-effector for attenuating the occurrence of the singularity. The performance is evident, as shown in Fig. 5. The collision-free path finding algorithm was performed in the Webot virtual simulation environment to validate different designs and application scenarios of the model robot's action when encountering obstacles in the workspace. Finally, the algorithm was implemented in an actual or physical system. The actual robotic arm movements were identical to the simulated results. The contribution of this paper is indicating valuable guidelines for 7-DOF humanoid robotic arm design, control, and path planning to make teleoperation or the autonomic robot arm movement more feasible instead of complex pre-setting and teaching by users.

ACKNOWLEDGMENT

The authors appreciate the support from the Ministry of Science and Technology of Taiwan under the grants 108-2218-E-007 -025 for the work described herein.

REFERENCES

- [1] N. Robson, "Simplified kinematic structure of the human arm" online available in https://www.researchgate.net/publication/280493078_ EXPERIMENTAL_OBSERVATIONS_ON_HUMAN_REACHING M OTION_PLANNING_WITH_AND_WITHOUT_A_REDUCED_MOBI LITY/figures.
- [2] KINOVA, "Jaco Assistive Robotic Arm" online available in https://www.kinovarobotics.com/en/products/assistivetechnologies/kinova-jaco-assistive-robotic-arm.
- [3] KUKA, "LBR iiwa" online available in https://www.kuka.com/zh-BA%E7%B3%BB%E7%B5%B1/industrial-robots/lbr-iiwa.
- [4] U. ROBOTS, "UR5" online available in https://www.universalrobots.com/tw/%E7%94%A2%E5%93%81/ur5/.
- Kiev, "Gimbal lock problem," 2011. Online available in http://3dvrm.com/quat/.
- [6] C. Chu, J. Xu, and C. Lan, "Development of a compact wrist mechanism with high torque density," in 2012 IEEE/ASME International Conference on Advanced Intelligent Mechatronics (AIM), 11-14 July 2012 2012, pp. 226-231, doi: 10.1109/AIM.2012.6265968.
- J. Grasshoff, L. Hansen, I. Kuhlemann, and K. Ehlers, "7dof hand and arm tracking for teleoperation of anthropomorphic robots," in Proceedings of ISR 2016: 47st International Symposium on Robotics, 2016: VDE, pp. 1-
- [8] D. N. Nenchev, Y. Tsumaki, and M. Takahashi, "Singularity-consistent kinematic redundancy resolution for the S-R-S manipulator," in 2004 IEEE/RSJ International Conference on Intelligent Robots and Systems (IROS) (IEEE Cat. No.04CH37566), 28 Sept.-2 Oct. 2004 2004, vol. 4, pp. 3607-3612 vol.4, doi: 10.1109/IROS.2004.1389975.
- [9] M. Shimizu, H. Kakuya, W. Yoon, K. Kitagaki, and K. Kosuge, "Analytical Inverse Kinematic Computation for 7-DOF Redundant Manipulators With Joint Limits and Its Application to Redundancy Resolution," IEEE Transactions on Robotics, vol. 24, no. 5, pp. 1131-1142, 2008, doi: 10.1109/TRO.2008.2003266.
- [10] P. Lozano, "Spatial Planning: A Configuration Space Approach," IEEE Transactions on Computers, vol. C-32, no. 2, pp. 108-120, 1983, doi: 10.1109/TC.1983.1676196.

- [11] R. A. Brooks and T. Lozano-Pérez, "A subdivision algorithm in configuration space for findpath with rotation," IEEE Transactions on Systems, Man, and Cybernetics, vol. SMC-15, no. 2, pp. 224-233, 1985, doi: 10.1109/TSMC.1985.6313352.
- [12] S. Ki and J. Hollerbach, "Local versus global torque optimization of redundant manipulators," in Proceedings. 1987 IEEE International Conference on Robotics and Automation, 31 March-3 April 1987 1987, vol. 4, pp. 619-624, doi: 10.1109/ROBOT.1987.1087955.
- [13] Y. Nakamura, H. Hanafusa, and T. Yoshikawa, "Task-Priority Based Redundancy Control of Robot Manipulators," The International Journal of Robotics Research, vol. 6, no. 2, pp. 3-15, 1987/06/01 1987, doi: 10.1177/027836498700600201.
- [14]D. N. Nenchev, "Redundancy resolution through local optimization: A review," Journal of robotic systems, vol. 6, no. 6, pp. 769-798, 1989.
- [15] T. Yoshikawa, "Manipulability of Robotic Mechanisms," The International Journal of Robotics Research, vol. 4, no. 2, pp. 3-9, 1985/06/01 1985, doi: 10.1177/027836498500400201.
- [16] C. Ericson, Real-Time Collision Detection, CRC Press, Inc., 2004, p. 632. [17] C. Jen-Hui and N. Ahuja, "An analytically tractable potential field model of free space and its application in obstacle avoidance," IEEE Transactions on Systems, Man, and Cybernetics, Part B (Cybernetics), vol. 28, no. 5, pp.
- [18] ROBOTIS, "Dynamixel Pro Motor," 2014. [Online]. Available: http://www.smart $robot.com.tw/mobile/product_d.php?lang=tw\&tb=1\&id=45\&cid=21.$

729-736, 1998, doi: 10.1109/3477.718522.



Yi-Hao Zhu received the B.S. and M.S. degrees in mechanical engineering in 2018 and 2020, respectively, from the Department of Power Mechanical Engineering, National Tsing Hua University, Hsinchu City, Taiwan. His research interest is the mechatronics system of the humanoid manipulator.



Hsien-Ting Chang received a B.S. degree in 2014 from the National Tsing Hua University, Taiwan, and M.S. degree in 2016 from National Tsing Hua University, Taiwan, all in mechanical engineering. Since 2016, he has been working toward a Ph.D. degree at National Tsing Hua University. His research interest is associated with motion capture, robot, and motion control, especially in signal processing and mechatronics integration.



Jen-Yuan Chang received the B.S. degree from the National Central University, Taoyuan City, Taiwan, in 1994, and the M.S. and Ph.D. degrees from Carnegie Mellon University, Pittsburgh, PA, USA, in 1998 and 2001, respectively, all in mechanical engineering. Dr. Chang is currently a Distinguished Professor with the Department of Power Mechanical Engineering, National Tsing Hua University, Hsinchu City, Taiwan and was an American Society for Engineering Research Education/National

(ASEE/NRC) Faculty Research Fellow with the U.S. Air Force Research Laboratory in Dayton, OH, USA. He worked at various R&D posts for highend magnetic disk storage devices with IBM and HGST in San Jose, CA, USA. Dr. Chang's researches in vibrations, mechatronics, and robotics have been recognized internationally including the American Society of Mechanical Engineers-Information Storage and Processing Systems (ASME-ISPS) Distinguished Institution Award, Outstanding Contribution Award, and MOST Outstanding Research Award and leadership services as the Division Chair of ASME ISPS Division, and the Vice Chair of Strategic Planning Committee. He is a member of Technical Committee of IEEE Magnetics Society and has served as Technical Editor and Associate Editor for IEEE/ASME Transactions on Mechatronics, ASME Journal of Vibration and Acoustics, Elsevier Mechatronics, and Springer Microsystems Technologies journals, He is a Fellow of ASME, CSME, RST and STAM.